COBEM 2021 26th International Congress of Mechanical Engineering
ABCM Associação Brasileira de Engenharia e Ciências Mecânicas
November 22-26, 2021, Virtual Congress, Brazil

COB-2021-1126
A FIRST-PRINCIPLES MODEL FOR AXIAL FANS: OPTIMIZATION RESULTS OF BLADE PITCH ANGLE

Gabriel Longen Podgaietsky
POLO Laboratories, Department of Mechanical Engineering, Federal University of Santa Catarina, Florianópolis, SC, Brazil
gabriel.longen@polo.ufsc.br

Marcelo De Lellis Costa de Oliveira
Department of Automation and Systems Engineering, Federal University of Santa Catarina, Florianópolis, SC, Brazil

Adriano F. Ronzoni
Nidec Global Appliance, 89219-521, Joinville, SC, Brazil

Christian Johann Losso Hermes
POLO Laboratories, Department of Mechanical Engineering, Federal University of Santa Catarina, Florianópolis, SC, Brazil

Abstract. *Aiming at designing more efficient components for refrigeration systems, a first-principles axial fan model is put forward in this paper, consisting of a discretization of the blade along the radial direction. At each element a sum of forces is performed considering the aerodynamic behavior of the blade section, besides the conservation of momentum. The resulting set of non-linear algebraic equations is solved iteratively through a sub-relaxation procedure. Numerical results based on an 8-inch 5-bladed condensing unit fan at 1350 RPM showed that the model reproduces well the head and shaft power trends observed experimentally, albeit overestimating these quantities within 10% and 20% bounds, respectively. To illustrate the model potential for design purposes, the pitch angle distribution of the baseline fan was optimized for 0 Pa and 10 Pa. The numerical results showed the optimized fans to be about 3% more efficient than the baseline one.*

Keywords: *axial fan, modeling, blade element theory, pitch angle optimization, characteristic curve.*

1. INTRODUCTION

Low pressure axial fans are widely used in condensing and evaporating units for domestic and commercial refrigeration. In the case of condensers, the power consumed by the fan directly affects the electric energy consumption of the product. For the evaporators the effect is twofold, since besides drawing electric power, the fan acts as a thermal load in the refrigerated compartment. Therefore, the development of more efficient refrigeration systems must also include the optimization of axial fans, that should be able to provide the required airflow at the lowest possible shaft power.

In general, the development of axial fans has been carried out experimentally, in a trial-and-error fashion, through standardized tests in a wind tunnel. Thereby the characteristic performance curves are obtained, which express the static pressure (head) and the fan efficiency as a function of the volumetric flow in a log-log diagram (ASHRAE, 1992). Recently, the improvement of computational fluid dynamics (CFD) has allowed a better understanding of the phenomena associated with the airflow over the fan blades, such as formation and detachment of the boundary layer, as well as leaks and reverse flow at the ends of the blade. However, CFD models have a high computational cost, thus hindering their use not only to analyze the sensitivity of the variables of interest in relation to specific design parameters, but mainly for optimization purposes, for which many combinations of geometric must be considered (Beiler and Carolus, 1999).

In contrast, models based on the fundamental principles of fluid mechanics can be employed to obtain a better understanding of the cause-effect relationships between the fan variables of interest and the design parameters, in addition to being a computationally faster way to obtain the characteristic curves. However, such models are scarce in the open literature, which is more focused on the simulation of wind turbines (Schubel and Crossley, 2012) and thrusters (Wallis, 1961). Thus, in the present work, a model for the simulation of axial fans is put forward based on the tripod formed by the blade element theory (Houghton and Carpenter, 2003), the aerodynamic characteristics of the airfoil Drela (1989) and the momentum conservation in the interaction of the flow with the fan (Castegnaro, 2017).

The rest of the paper is organized as follows. In the next section the fan mathematical model is presented, followed by the proposal of a solution algorithm. To cope with current limitations in the model, an extrapolation strategy for the generation of the performance curves is proposed. To illustrate the design potential of the developed model, an

optimization of the blade pitch angle of a given condenser fan is presented.

2. SIMULATION MODEL

In the sequel the three pillars of the axial fan model advanced in this paper will be briefly discussed, followed by a consideration on the radial flow and the parameterization of a condensing unit fan used as a study case.

2.1 Blade Element Theory

The blade element theory (BET) was originally developed for the analysis and design of aeronautical propellers Houghton and Carpenter (2003). It consists basically of a discretization of the blade along the radial direction. The idea here was to adapt this approach to the impellers case. In Fig. 1 it is shown a blade profile (airfoil) obtained by intersecting the red cylinder shell of radius r with the fan blades. The blade element is obtained by considering a finite size δr centered at the r coordinate. As the fan rotates at angular speed Ω, an axial flow is created with a speed V_a as well as a tangential flow with speed $\Omega r(1-b)$ relative to the blades, where $0 < b < 1$ is the so-called induction coefficient. The vector sum of the axial and tangential flows produces a resulting flow V_r with an angle of attack α with respect to the chord line, which is a straight line passing through the leading and trailing edges of the airfoil. The line segment c between them is the chord length. The latter forms a pitch angle θ with respect to the plane of rotation. The angle between the resulting flow and the plane of rotation can be calculated from:

$$\phi = \arctan\left(\frac{V_a}{\Omega r(1-b)}\right). \tag{1}$$

Once determined, it can be used for the calculation of the resulting flow speed, as follows:

$$V_r = \frac{V_a}{\sin\phi}. \tag{2}$$

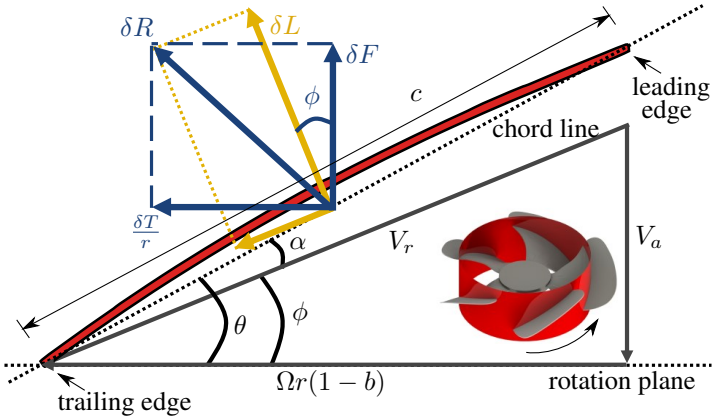

Figure 1: Parameters involved and forces acting upon a blade section (airfoil).

2.2 Momentum Conservation

Castegnaro (2017) stated that the average force imposed by the fan on the axial flow is comprised of two parts, namely the difference of static pressure between the inlet and outlet of the fan, Δp_e, and the dynamic pressure at the outlet of the fan, $(1/2)\rho V_a^2$, with ρ being the air specific mass. The same idea can be applied locally. By applying Bernoulli's principle to a streamline that goes through the blade element, it is possible to compute the local axial flow velocity from:

$$V_a = \sqrt{\frac{2}{\rho}\left(\frac{F}{S} - \Delta p_e\right)}. \tag{3}$$

Also, as done by Houghton and Carpenter (2003), assuming that far upstream and far downstream the angular flow speed is 0 and $2b\Omega$, respectively, considering a linear behavior in between and knowing that δQ is the volumetric flow, by applying the principle of momentum conservation it is possible to demonstrate that the torque δT at the element is

$$\delta T = \rho(2b)\Omega r^2(\delta Q). \tag{4}$$

2.3 Airfoil Theory

The forces of aerodynamic lift, δL, and drag, δD, are defined as follows:

$$\delta L = \frac{1}{2}\rho V_r^2 C_l \delta S \tag{5}$$

$$\delta D = \frac{1}{2}\rho V_r^2 C_d \delta S, \tag{6}$$

where C_l and C_d are the coefficients of lift and drag, respectively, and δS is the total blade element area considering all blades. By performing the sum of forces in the axial and tangential directions one gets

$$\delta F = \frac{1}{2}\rho V_r^2 \left(C_l \cos\phi - C_d \sin\phi\right) \delta S \tag{7}$$

$$\frac{\delta T}{r} = \frac{1}{2}\rho V_r^2 \left(C_l \sin\phi + C_d \cos\phi\right) \delta S. \tag{8}$$

The performance of the blade sections is described using the XFOIL model Drela (1989). Given a certain shape, XFOIL predicts the drag and lift coefficients of the airfoil as a function of the attack angle and the Reynolds number, calculated from $R_e = cV_r/\nu$, where ν is the air kinematic viscosity. As XFOIL does not provide continuous results allover the domain, a multivariate polynomial regression was performed to fill in the gaps. For illustration purposes, the results for one of the scanned blade profiles of a given condenser fan are shown in Fig. 2.

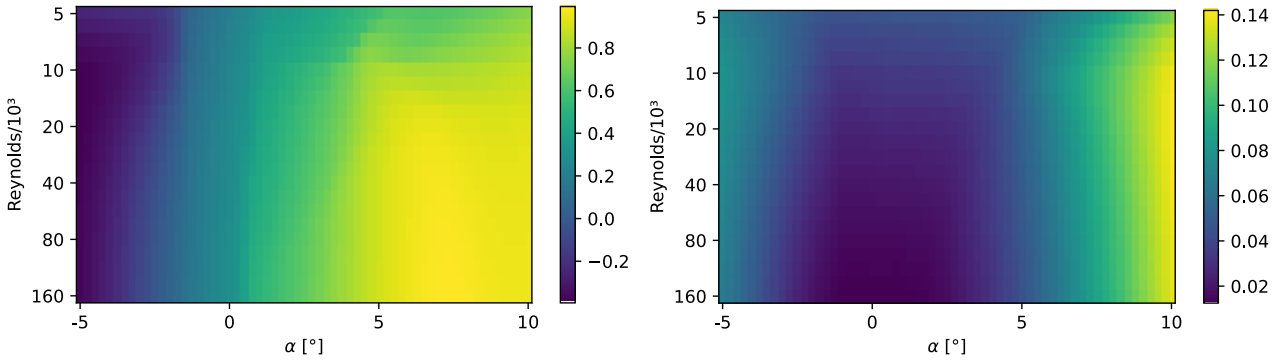

(a) Lift. (b) Drag.

Figure 2: Interpolated aerodynamic coefficient maps of a scanned blade profile: (a) lift and (b) drag coefficients.

2.4 The Zero Radial Air Flow Assumption

When considering axial fans working at a low static pressure difference (head), which is usually the case for refrigeration systems, the radial flow should be negligible. This means that, according to Downie *et al.* (1993), the radial pressure gradient must balance the centrifugal force, so that

$$\frac{1}{\rho}\frac{\delta P_r}{\delta r} = \frac{V_t^2}{r}, \tag{9}$$

where $V_t = 2\,b\,\Omega$ is the flow tangential velocity and δP_r is the radial pressure difference over the element of size δr. Thus, assuming that the static pressure distribution upstream of the fan is uniform, given the absence of a preswirl, through the downstream pressure distribution it is possible to determine the pressure difference imposed on each element. Based on the considerations on the tangential flow behavior already made, it is possible to rewrite Eq. 9 to express the radial pressure difference in the downstream plane as a function of the model variables:

$$\delta P_{rd} = \rho r (2b\Omega)^2 \delta r. \tag{10}$$

To allow the computation of the radial pressure gradient, it was necessary to create a staggered mesh with respect to the flow (blade element) mesh, as depicted in Fig. 3, in which r_0 and R are the hub and rotor radius, respectively. Also illustrated are the static pressure radial distributions: the upstream one has a negative distribution due to tunnel head loss and with a value decreasing from hub to tip due to the increase of velocity V_a (usually proportional to radius), whereas the downstream one depends linearly on the radius (although b may vary with r). For the sake of illustration it was assumed that the fan discharges at the atmosphere, which is the case for wind tunnel tests. Hence $\int p_e(r)dr = 0$ must be satisfied, which means that $p_e(r)$ must cross zero at some point. The overall static pressure difference, Δp_e, over each blade element (flow point) is taken as the mean value between the two neighboring pressure difference points.

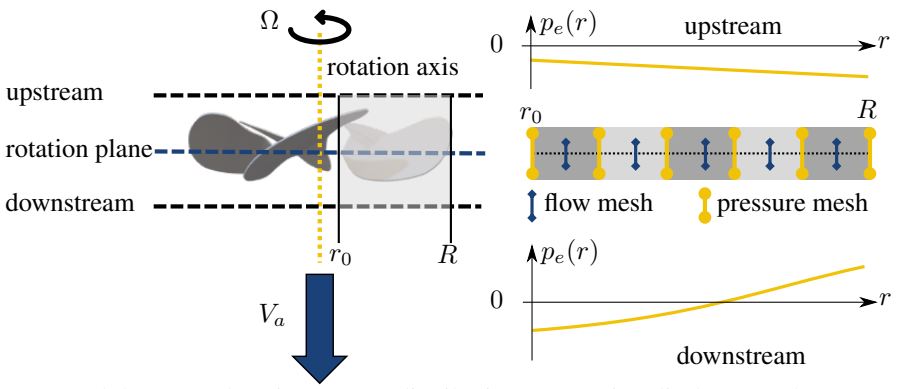

Figure 3: Mesh layout and static pressure distributions (assuming discharge at the atmosphere).

2.5 Model Parameterization

The model described so far aims to determine the performance of an axial fan given geometric and operation inputs. The main model parameters (inputs), as well their values for a given fan of a condensing unit which will be used for numerical and experimental results further on, are summarized in Tab. 1. Values described as "mean" denote parameters that may change with the radial coordinate.

Table 1: Main model inputs (parameters).

Description	**Symbol**	**Analyzed fan value**
Hub radius	r_0	31.24 mm
Blade (rotor) radius	R	97 mm
Number of blades	N_p	5
Chord length	c	65.29 mm (mean value)
Blade pitch angle	θ	27.35 deg (mean value)
Lift and drag coefficients	C_l and C_d	XFOIL lookup table
Rotor angular speed	Ω	1350 RPM
Global static pressure difference	Δp_e	(varied, imposed by wind tunnel)
Air density	ρ	$1.205\,\mathrm{kg/m^3}$
Air kinematic viscosity	ν	$1.511 \cdot 10^{-5}\,\mathrm{m^2/s}$

3. SOLUTION ALGORITHM

Since a closed solution for the non-linear model cannot be found, an iterative numerical procedure must be carried out for each of the blade elements. Once the solution variation among adjacent iterations become negligible, the problem is solved and the fan flow and torque are obtained by integrating the contribution of each element along the radial direction. The algorithm flowchart is presented in Fig. 4. It starts by imposing a uniform pressure distribution downstream of the fan. The algorithm enters a profile loop at the outer radius, where the buoyancy force is greater and therefore a numerical solution is easier to obtain. Initially, the values of V_a and b are arbitrated, which allow for the Reynolds number and the value of α to be computed through Eqs. (1) and (2). Thereby the values of C_l and C_d are retrieved from the lookup table previously obtained from XFOIL. Next the values of thrust and torque are computed through Eqs. (7) and (8). Finally through the equations (3) and (4) the new values of V_a and b are obtained. If the difference between these values and those of the previous iteration is within a certain tolerance, the solution is considered found and the algorithm moves on to the next blade element, updating the value of the next element in the pressure mesh through Eq.(10). Otherwise, the solution values are under-relaxed for a next iteration. The algorithm ends when all blade elements are processed or

when an element becomes insoluble, that is, its solution cannot be computed. The insolubility starts at some inner blade element, and moves outward in the radial direction as the fan head is increased. This problem may stem from the fact that the aerodynamic curves currently obtained with XFOIL are only representative for blade profiles up to an angle of attack of about 8° for such extremely thin airfoils. It is believed that, with a more precise computation of the aerodynamic curves, it will be possible to solve all blade elements. Once the profile loop is concluded, possibly preempted by an insoluble element, a pressure distribution correction is performed in an attempt to make the integration of the elements of this mesh equal to the global static pressure difference, Δp_e, imposed as input. The pressure distribution and those of other variables are then evaluated and it is determined whether the variations between iterations is within a desired tolerance. If not, the profile is solved once more, this time starting with the pressure distribution just computed. In general, the model takes about four iterations to converge. Once it does so, a post-processing is performed, where the axial flow and torque radial distributions are integrated to determine, mainly, the axial airflow and shaft power consumed by the fan.

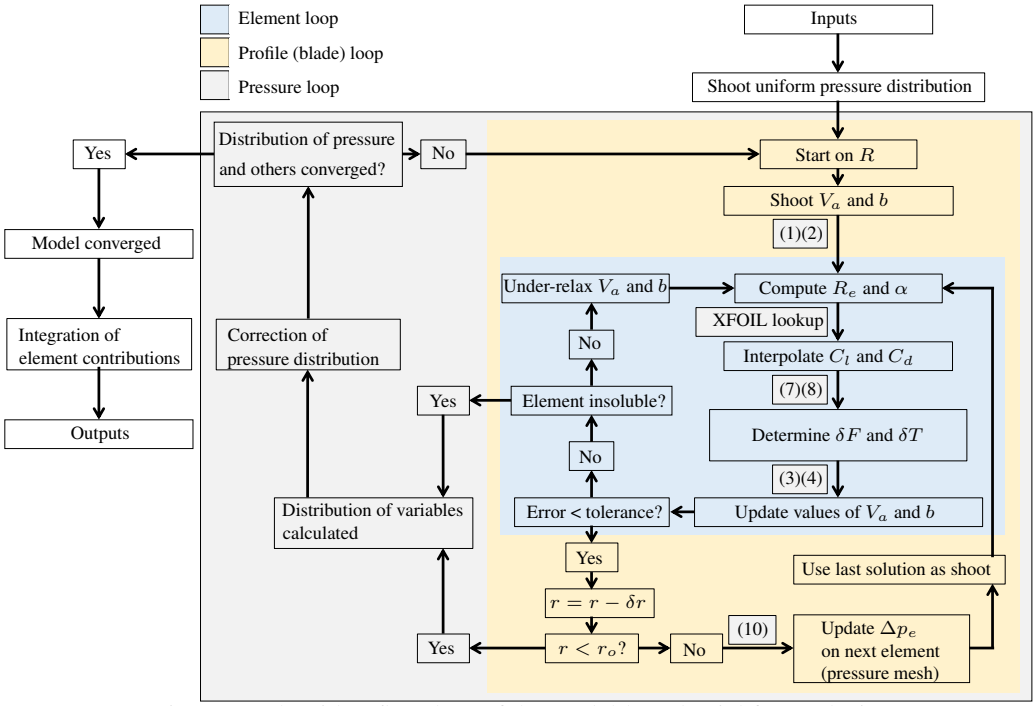

Figure 4: Algorithm flowchart of the model-based axial fan analysis.

4. FLOW AND POWER CORRECTION

During preliminary tests with the model it was observed that the amount of unresolved internal elements increased with the fan head. Thus, an increasing loss of information took place when attempting to compute the characteristic curves of the fan, for which Δp_e must be varied. Thus, a strategy for correction of the calculated flow based on the insolvency point was elaborated. Note that this is only a palliative solution for evaluating the model with the specific analyzed fan at this stage of the research. The correction assumes a linear variation in the axial velocity, starting from zero at $r = r_0$ to the value observed at $r = R$. This hypothesis can be verified in Fig. 5, where the radial distribution of axial velocity for two head values is shown. For the 20 Pa case the insolvency point is located just above $r = 60$ mm. By observing both head scenarios, it is possible to conclude that the linear velocity distribution hypothesis seems reasonable. It also relies on the fact that the particular studied fan has a practically uniform pitch distribution, which results in V_a being, for outermost larger rotor part, a linear function of the radius. Assuming the linear velocity variation, it is possible to work with a normalized radial coordinate, r^*, to more easily integrate the velocity field within the span of interest and determine an expression for the sum of axial flow within it. The normalized radius is computed in a way that it assumes the values 0 and 1 at r_0 and R, respectively:

$$r^* = \frac{r - r_0}{R - r_0}. \tag{11}$$

The axial volumetric flow can be obtained by integrating the product between the axial velocity and an area differential:

$$\dot{V} = \int V_a dA. \tag{12}$$

Based on the assumption of linear velocity distribution one can write $V_a = V_{a,\max} r^*$, where $V_{a,\max}$ is the maximum value of the V_a distribution, observed at $r^* = 1$. The area differential in polar coordinates can be written as $dA = 2\pi r dr$. The radius differential, in turn, can be expressed as a function of its normalized counterpart by differentiating Eq. (11), yielding $dr = dr^*(R - r_0)$. By replacing these expressions into Eq. (12), ones gets

$$\dot{V}_i = \int_0^{r_p^*} r^* \left[r^*(R - r_0) + r_0 \right] (R - r_0) dr^*, \tag{13}$$

where r_p^* is the normalized radius at which the integration should stop, i.e. the insolvency point. By performing the integration, the extrapolated volumetric axial flow within the insolvent part of the rotor is

$$\dot{V}_i = 2\pi V_{a,\max} (R - r_0) r_p^* \left[\frac{(R - r_0) r_p^*}{3} + \frac{r_0}{2} \right]. \tag{14}$$

On the other hand, if Eq. (13) is integrated within the normalized span delimited by r_p^* and 1, one gets the volumetric axial flow of the solved part of the rotor, $\dot{V}_s$. Hence, a ratio between these flow shares can be defined:

$$\kappa = \frac{\dot{V}_s}{\dot{V}_i} = \frac{(1 - r^{*3}) \frac{(R - r_0)}{3} + (1 - r^{*2}) \frac{r_0}{2}}{r^{*2} \left[\frac{(R - r_0) r^*}{3} + \frac{r_0}{2} \right]}. \tag{15}$$

Hence, once the value of κ is computed, the estimated total axial flow of the fan can be calculated as:

$$\dot{V} = \dot{V}_s \frac{1 + \kappa}{\kappa}. \tag{16}$$

For the shaft power correction, the same extrapolation idea is applied although considering that the power varies not linearly but with the square of the radius.

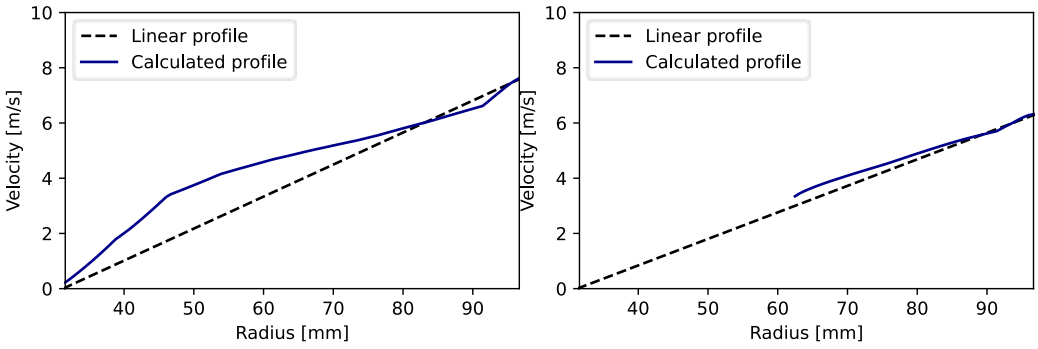

(a) $\Delta p_e = 0$ Pa (free flow). (b) $\Delta p_e = 20$ Pa.

Figure 5: Computed axial velocity distribution as a function of the fan head.

5. PITCH ANGLE OPTIMIZATION

As an optimization exercise it was decided to determine the optimal pitch angle θ distribution, since it has a great impact on the fan performance. The optimization was carried out for 0 Pa and 10 Pa head values, at which a few elements are insoluble. Aiming at a wide optimization domain, a routine was created covering all possible θ distributions, which can only be evaluated in a relatively short time thanks to the low computational cost of the model. The process starts with a discretization of the blade in just 4 elements, for faster convergence. The fan parameterization is the same as that in Tab. 1, except for θ, which is varied from 10° to 50° in steps of 2.5° for a total of 17 steps. All pitch values of all elements are combined between one another, yielding $17^4 = 83,521$ possible distributions to be simulated, and their corresponding values of flow and shaft power to be computed. The pitch profile chosen as optimal is the one that delivers at least the same axial flow as the baseline (existing) fan at the lowest power consumption. Once the optimal pitch profile is determined, the blade is re-discretized, this time in 5 elements. The 4-element pitch profile is linearly interpolated to 5 points, with the pitch angle at both ends of the 4- and 5-element profiles having the same value. The process described in the previous

paragraph is performed once more, except that now θ is varied in each element by 3° up to a maximum distance of 12° from the starting 5-element distribution in both directions. Thus, the combination of all possible θ distributions results now in $9^5 = 59,049$ simulations, after which the same decision criterion is applied. This winning distribution now serves as the basis for a new iteration with 5 elements, but this time with θ steps of 2° up to a maximum distance of 8°. The process is repeated again with a variation of 1° up to a maximum distance of 4°, and then the optimum θ profile for a 5-element blade is settled. This process is repeated for a discretization into 6, 7, and 8 elements, totaling 867,673 simulations. With the optimal profile defined for 8 elements, it is considered that the pitch optimization routine is finished. It should be noted that for this optimization process all element inputs are kept constant, except for Δp_e and, obviously, θ. Thus, as the element outputs become a function of only 3 inputs, namely the triple $(r, \theta, \Delta p_e)$, it was decided to generate a large lookup table with the pre-calculated outputs. Note that it is still necessary to make the static pressure field converge, but by using the lookup table the optimization is greatly accelerated as all element solutions are already available. In this way, it is possible to carry out all the 867,673 simulations in less than 1 hour. In Fig. 6 the output maps for the outermost radius in an 8-element discretization are shown. The insolubility region is colored in gray. In the efficiency map, defined as the thrust times the axial velocity divided by the shaft power of the element (torque times angular speed), an interesting trend can be observed: as Δp_e increases, the efficiency peak is found at lower pitch angles.

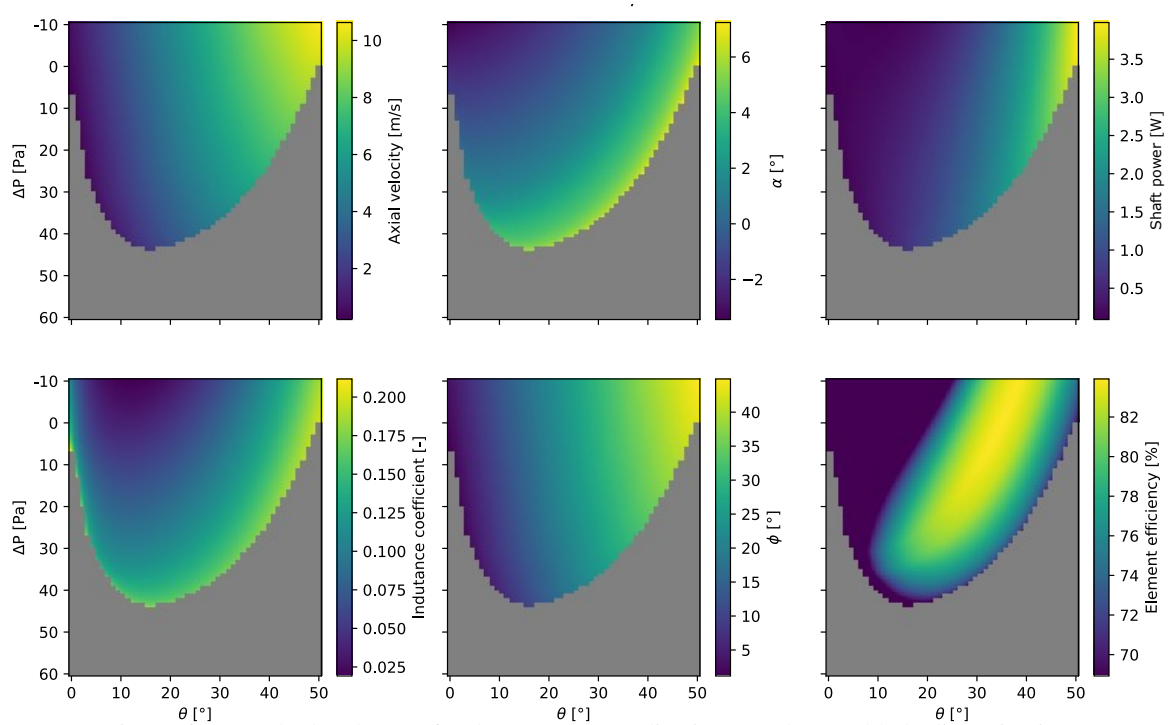

Figure 6: Pre-calculated maps for the outermost radius in an 8-element blade discretization.

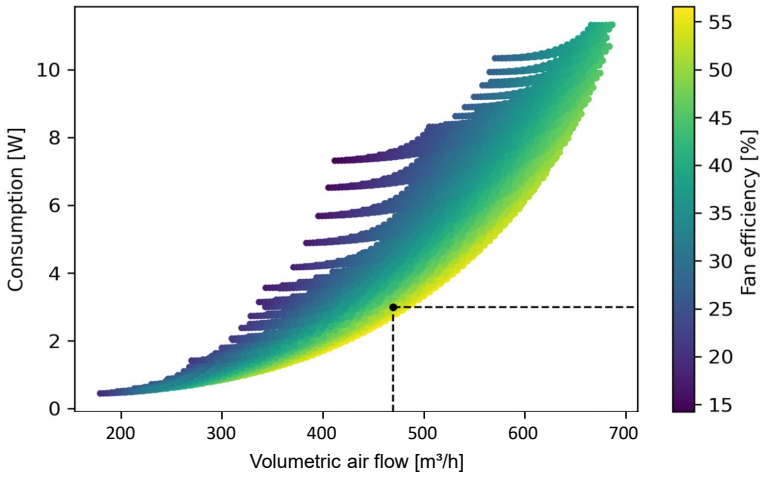

Figure 7: Pareto map for a 4-element blade optimization at free flow.

In Fig. 7 it is shown the results for all 4-element θ profiles for the free flow condition ($0\,Pa$). The dots are colored according to the efficiency value of each profile, defined by Castegnaro (2017) as the ratio between the total pressure difference (static more dynamic) times the fan flow, and the consumed power. In the figure, it can be seen that there is a Pareto front, where the points have greater efficiency, suggesting that the proposition of this indicator seems adequate. In addition, from the baseline point (black dot) on the graph it can be noted that, if keeping the flow constant, the shaft power can be reduced by 7.1%; whereas if the power (torque) is the one kept constant, the flow can be augmented by 2.0%.

6. RESULTS

In the sequel, model validation results based on wind tunnel tests will be discussed at first, followed by pitch angle optimization results.

6.1 Model Validation

To validate the model, the characteristic curves of fan head and shaft power as a function of the flow were compared against the curves obtained experimentally in a wind tunnel, as can be seen in Fig. 8. Looking at the Δp_e curve, it is clear that up to 10 Pa the model captures quite well the experimental trend, within a threshold of 10%. The overestimation in the flow for a same head is most likely due to the fact that the model still not considers non-idealities such as blade tip losses, heat dissipation and flow disturbance inter blades.

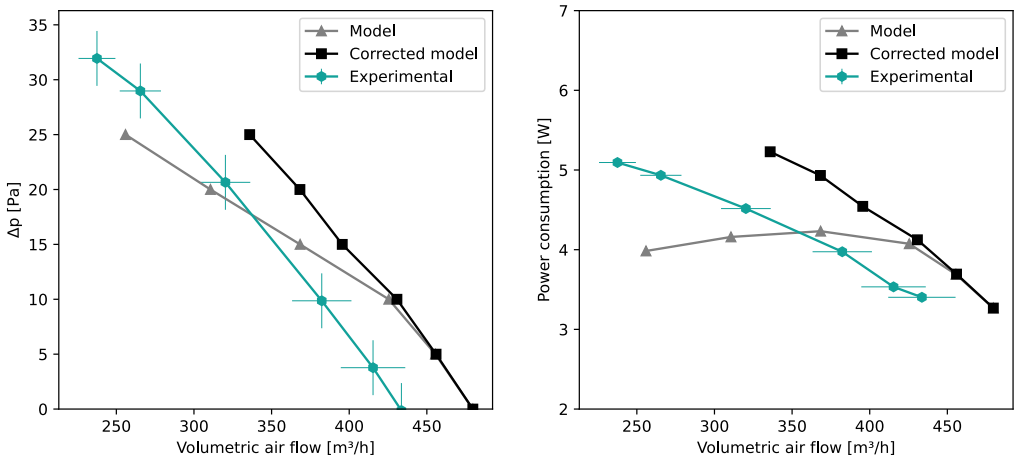

Figure 8: Validation results of the model with and without correction against wind tunnel results.

Nonetheless, for $\Delta p_e > 10$ Pa the model fails to continue reproducing the experimental trend, as the number of insoluble elements grows. To cope with this limitation it was applied the model correction (extrapolation) strategy, as explained in section 4. Note how the resulting curve continues to reproduce well the experimental trend above 10 Pa. The same behavior is observed for the power consumption curves, with the corrected model curve capturing quite well the experimental power consumption, although within a 20% error margin. By crossing information from both graphs in Fig. 8, it is possible to observe that, for a given Δp_e (e.g., 10 Pa), the corrected model is capable of generating more volumetric flow (about 15% more) at roughly the same shaft power, for the lack of modeled non-idealities already explained.

6.2 Pitch Angle Optimization

The pitch angle distributions determined in the optimization process for head values of 0 Pa and 10 Pa are shown in Fig. 9. The gray area represents the allowed region in which θ can be chosen based on manufacturing constraints. Note in the figure that the baseline profile has a reasonably constant θ for about 2/3 of the rotor, with $r > 50$ mm, and that the optimized distributions tend to have higher internal and lower external θ values. This is because with the optimized θ distribution there is a more uniform V_a field, reducing the power consumption for the same flow, since for concentrated speed distributions (usually larger at the blade tips) the power consumption grows faster with the radius than the flow.

In Fig. 10 the fan characteristic curves obtained with the model for the pitch angle distributions in Fig. 9 are presented. Note that for the Δp_e (head) curve, the optimized distributions yield results very close to the baseline case, especially at the points for which they were optimized. However, it can be seen that for a given flow value, obtained at roughly the same head value for all 3 analyzed cases, both optimized profiles draw less shaft power than the baseline one, which can be interpreted as a design gain. This can be attributed to a more uniform axial velocity distribution as a result of the optimized θ, as already mentioned. Finally, in the right-hand side graph the fan efficiency as formulated by Castegnaro (2017) is shown, corroborating the intuition of a slightly more efficient fan with the optimized blade profiles.

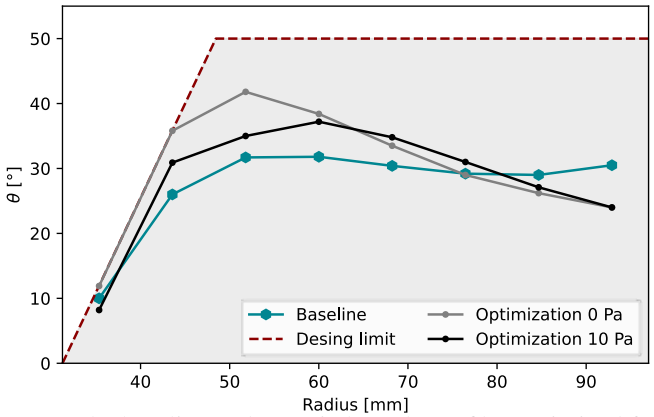

Figure 9: Comparison among the baseline and two pitch angle profiles optimized for different head values.

With the purpose of validating the optimization, two fans were prototyped through a 3D printing process: the baseline fan design and the one with the θ distribution optimized for 10 Pa. In Fig. 11 the characteristic curves for both fans obtained through wind tunnel experiments are presented. It can be seen in the left-hand side graph that their head versus flow behavior is very similar, with perhaps the optimized fan producing a slighter weaker flow for larger head values. However, it can be seen that, given the same flow, the optimized fan draws slightly less power than the baseline one. Putting these two counteracting trends together results in the behavior seen in the right-hand side graph, as expected: no clear distinction between both fan efficiencies can be drawn.

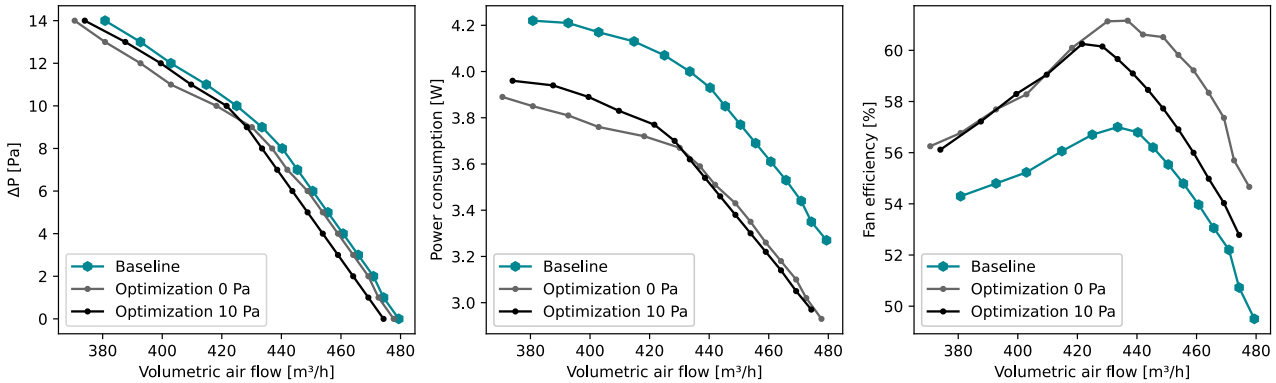

Figure 10: Fan characteristic curves obtained with the model for the baseline and optimized pitch angle profiles.

Back to Fig. 11, note that the reduction in the power consumption of the optimized fan, although small, is maintained throughout the whole curve. This suggests that the reduction represents reality and is not an experimental error. Also, by comparing the Figs. 10 and 11 one concludes that the consumption reduction observed experimentally is relatively smaller than the numerical one. This can be explained by the fact that the parameterization, design, and specially the manufacturing process of the fans in the laboratory is still incipient. It is expected that, with the improvement of these processes, blades with significantly greater efficiencies will be obtained in practice.

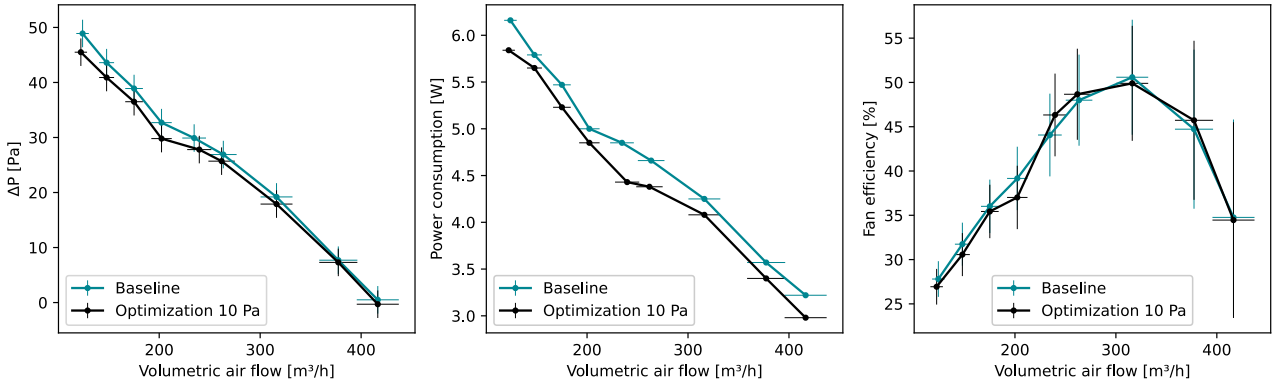

Figure 11: Fan characteristic curves obtained with wind tunnel experiments for the baseline and the optimized fans.

7. CONCLUSION

Aiming at designing more efficient components for refrigeration systems, in this paper a first-principles model of an axial fan was put forward, consisting basically of a discretization of the blade along the radial direction. At each element a sum of forces is performed considering the aerodynamic behavior of the blade section, besides the conservation of momentum. The result is a non-linear algebraic set of equations, which is solved iteratively through an under-relaxation numerical procedure. Given as input the fan head and speed, as well as blade geometry parameters and the curves of aerodynamic lift and drag, the solution algorithm also determines the downstream pressure distribution. Once the algorithm has converged, the element contributions of axial flow velocity and torque are integrated for the computation of the fan volumetric flow and shaft power. To cope with current model limitations that do not allow for a solution to be found for some inner elements, a fan flow and power correction strategy based on linear extrapolation of the axial speed distribution was proposed.

Numerical results based on an 8-inch 5-bladed condensing unit fan at 1350 RPM showed that the corrected model reproduces well the behavior observed in wind tunnel tests, although overestimating the fan head and power consumption within a 10% and 20% error margin, respectively. This resulted in a 15% more efficient modeled fan in comparison to the real (baseline) one, which was already expected since non-idealities such as blade tip re-circulation, heat dissipation and inter-blade flow perturbation have not yet been taken into account. The model took about 1 hour to be solved in a 3.4 GHz processor computer, which characterizes several orders of magnitude acceleration with respect to the CFD approach.

To illustrate the potential of the model for design purposes, the pitch angle distribution of the baseline fan was optimized for 0 Pa and 10 Pa head values. The numerical results showed the optimized fans to be about 3% more efficient than the baseline one. However, when considering the 10 Pa optimized fan against the baseline one in wind tunnel tests, no clear distinction between them in terms of efficiency was observed. This may have happened due to limitations in the 3D scanning, design and, particularly, manufacturing processes in the laboratory.

As future work prospects, the non-idealities already mentioned will be incorporated into the model. Also, the aerodynamic coefficients will be recalculated in a more precise way, which should contribute to solving more blade elements that are currently insoluble. Finally, other geometric parameters such as the blade shape (airfoil) itself and the chord length will be optimized, at first separately, for later to be incorporated in a multivariate optimization along with the pitch angle.

8. ACKNOWLEDGEMENTS

This work was performed under the auspices of the National Institutes of Science and Technology (CNPq 404023/2019-3, FAPESC 2019TR0846). The authors are grateful for the financial support of Nidec/Embraco and Embrapii through grant No. PPOL-1901.0020.

9. REFERENCES

ASHRAE, 1992. "Standard methods for laboratory airflow measurement". Standard, American Society of Heating, Refrigerating and Air-Conditioning Engineers, Inc. Reaffirmation of ANSI/ASHRAE 41.2-1987 with minor editorial changes.

Beiler, M.G. and Carolus, T.H., 1999. "Computation and measurement of the flow in axial flow fans with skewed blades". *Journal of Turbomachinery*, Vol. 121, pp. 59–66. doi:10.1115/1.2841234.

Castegnaro, S., 2017. *An Aerodynamic Method to Design Low-Speed Axial Fans with Imposed Diameter and Rotor speed*. Ph.D. thesis, Universitá Degli Studi di Padova.

Downie, R.J., Thompson, M.C. and Wallis, R.A., 1993. "An engineering approach to blade designs for low to medium pressure rise rotor-only axial fans". *Experimental Thermal and Fluid Science*, Vol. 6, pp. 376–401. ISSN 0894-1777.

Drela, M., 1989. *XFOIL: An Analysis and Design System for Low Reynolds Number Airfoils*, Springer, Berlin, Heidelberg, Vol. 54 of *Lecture Notes in Engineering*. ISBN 978-3-540-51884-6. doi:10.1007/978-3-642-84010-4_1.

Houghton, E.L. and Carpenter, P.W., 2003. *Aerodynamics for Engineering Students*. Butterworth-Heinemann, 5th edition. ISBN 0750651113.

Schubel, P.J. and Crossley, R.J., 2012. "Wind turbine blade design review". *Wind Engineering*, Vol. 36, pp. 365–388. doi:10.1260/0309-524X.36.4.365.

Wallis, R.A., 1961. *Axial Flow Fans: Design and Practice*. Academic Press.

10. RESPONSIBILITY NOTICE

The authors are solely responsible for the printed material included in this paper.